Fusion Science and Technology

ISSN: 1536-1055 (Print) 1943-7641 (Online) Journal homepage: www.tandfonline.com/journals/ufst20

Investigations into Dust Waste Treatment for Nuclear Fusion

Thomas Stokes, William Grove , James Hall-Bromley , Daniella Heristchian & Stephen Reynolds

To cite this article: Thomas Stokes, William Grove , James Hall-Bromley , Daniella Heristchian & Stephen Reynolds (27 Jan 2026): Investigations into Dust Waste Treatment for Nuclear Fusion, Fusion Science and Technology, DOI: 10.1080/15361055.2025.2605607

To link to this article: https://doi.org/10.1080/15361055.2025.2605607

FUSION SCIENCE AND TECHNOLOGY

DOI: https://doi.org/10.1080/15361055.2025.2605607

Investigations into Dust Waste Treatment for Nuclear Fusion

Thomas Stokes, William Grove, James Hall-Bromley, Daniella Heristchian, and Stephen Reynolds
Culham Science Centre, United Kingdom Atomic Energy Authority, Abingdon, United Kingdom

Received July 17, 2025
Accepted for Publication December 13, 2025

Abstract — *The generation and accumulation of dust in decommissioning activities pose challenges related to safety, waste management, and environmental impact. This study details inactive trials for two treatment strategies for managing dust waste: high-temperature baking and metal melting. Thermal processing was first examined through thermal treatment trials, analyzing the oxidation and adhesion behaviors of ITER-relevant dusts under air and inert gas conditions. Trials in the Materials Detritiation Facility (MDF) tested the viability of using dust containment baskets to facilitate high-temperature processing while minimizing contamination spread. Parallel to this, metal melting via vacuum induction melting (VIM) was explored as a method for consolidating fine dusts into ingots, mitigating dispersal risks. The results of this work indicate that oxidation affects dust morphology, potentially influencing waste processing. Dust baskets in the MDF contained the dusts, although minor loss and agglomeration occurred. The VIM trials evidenced that fine dusts could be incorporated into ingots. The use of metal containers to seed melting was promising. Tungsten powders were incorporated into melts of stainless steel and Inconel, but presented challenges when mixed with copper. These findings contribute to the development of scalable, safe, and efficient strategies for handling dust wastes, supporting long-term waste management solutions for nuclear fusion.*

Keywords — *Tritium, fusion, dust, waste, dust waste.*

I. INTRODUCTION

Tritiated and activated metallic dusts and powders will be generated during waste processing of fusion facility components during size reduction and dismantling. The amount of dust produced will vary depending on the material type and cutting technique used [1–3], as well as the amount of size reduction needed for components to be disposed of or further treated.

In one study, for stainless steel (SS) using plasma cutting, between 0.6% to 5.7% of the starting mass was captured in dust filters during the cutting operation [2], with more dust, which was not captured, remaining in the cutting zone. Other cutting techniques displayed higher values still [3]. The size of these dusts is typically larger than that of in-vessel dust, ranging from (micron to millimeter scale depending on the cutting technique used [4].

With ITER utilizing a W and SS first wall, it is expected that significant quantities of tritiated and activated dust from these materials will be generated, amongst other metals.

Activated and tritiated dusts pose inhalation and ingestion hazards during handling and accidental release scenarios [5]. The fine particulate size and high surface area of these dusts increase the potential for environmental contamination if containment fails [6]. These risks apply primarily during processing or accidental release conditions rather than during final disposal. Therefore, it is of importance that strategies are developed to also manage the volume of fines that will be generated during operation and as part of decommissioning and waste management.

The Materials Detritiation Facility (MDF) [7], which is used routinely to treat solid waste via baking to reduce activity levels from intermediate-level waste (>12 kBq/g ^{3}H) to low-

CONTACT Thomas Stokes tom.stokes@ukaea.uk

level waste classification (<12 kBq/g ^{3}H), provides an operational platform to trial dust handling/containment approaches. Vacuum induction melting (VIM) is another method that enables melting and consolidation under vacuum/inert atmospheres, limiting oxide-barrier formation that can inhibit tritium release [8,9] while safely reshaping fines into consolidated ingots.

This paper reports on inactive, proof-of-concept trials of high-temperature baking of SS and W powders, including the use of mesh dust baskets to contain fines on an industrial scale and VIM to consolidate powders/swarf and determine seed-fraction thresholds for reliable inductive coupling.

II. METHODS

II.A. Pyrolyzer Heating

The effects of high temperatures on dusts were investigated to see if processes such as oxidation, sintering, partial melting, or fusing would take place during detritiation operations.

Dusts were purchased from Fischer Scientific (W ~12 µm, SS 316L ~44 µm). This work was undertaken in the United Kingdom Atomic Energy Authority's (UKAEA's) Tritium Analysis Laboratory (TAL) utilizing a Raddec 6-Trio pyrolyzer. The 5-g dust samples (uncompacted) were heated up to 900°C and held for 2 h in air and Ar (250 mL min^{-1}), before cooling.

Pre- and post-treatment masses were recorded, and imaging by scanning electron microscopy (SEM)/energy-dispersive spectroscopy (EDS) was undertaken. ImageJ was used to estimate the projected particle areas from thresholded SEM micrographs for selected fields of view. Both the diameter and area measurements were treated as qualitative indicators of morphology change. Limitations included particle overlap, variable contrast, and small sample sizes, which resulted in high variability.

These metrics were therefore used to support visual observations rather than to calculate oxide thickness or mass gain. For diameter measurements, five particles from each micrograph were randomly selected without bias toward size or position to provide a representative sample from each field of view. Raman was utilized for identification of the W oxide phases.

II.B. MDF Dust Basket Trials

The effectiveness of novel "dust baskets" in the MDF was tested on clean dust to determine if this methodology would be suitable for large-scale dust detritiation. The MDF routinely only accepts bulk metallic pieces, as opposed to dust, due to the furnace becoming a turbulent environment during processing. Therefore, any dust and chips loose in the furnace would be spread within the furnace.

Two cylindrical SS304 woven mesh baskets (seen in Fig. 1) were procured (1-µm and 5-µm pore size, 3-mm mesh thickness, ~650 mm × 168 mm), loaded with ~1 kg of SS316L powder (Fischer Scientific, SS316L, ~44 µm) and baked to 1000°C (350 L min^{-1}; 5°C min^{-1} ramp) before cooling over a period of approximately 6 h. The pre/post total masses of the basket and dust and observations following the heating process were recorded. The baskets had preexisting oxide scale from prior furnace use.

Each run was performed with a single replicate ($n = 1$).

II.C. Vacuum Induction Melting

The effectiveness of the VIM furnaces as a method for agglomerating clean samples representing particulate waste from fusion, including W dusts, was tested. A 4-kg capacity VIM furnace supplied by Consarc Engineering Ltd., with a 20-kW, 10-kHz power supply, was used in this trial.

The materials tested included SS swarf (millimeter scale, irregular shape), atomized SS316 powder (<45 µm, >25% Fe, >1% Cr, 10% to 24.99% Ni, >1% Mo, >1% Si, 0.1% to 0.99% Co), Cu granules (3 to 5 mm, 99.99% Cu material), and W powder (45 to 90 µm, >99.9% purity). For the W runs, approximately 20 wt% W was used.

The skin depth δ for induction heating is expressed in Eq. (1) [10], where ρ is resistivity, ω is angular frequency and μ is permeability,

Fig. 1. Images of the dust baskets used to treat the finely divided material.

$$\delta = \sqrt{\frac{2\rho}{\omega \times \mu}} . \quad (1)$$

Powders with a characteristic size much less than δ couple poorly and benefit from seed bulk that couples directly and transfers heat by conduction/stirring. For 10 kHz, the representative minimum δ are ~4.2 mm (SS304), 0.66 mm (Cu), and ~5.1 mm (Inconel 600).

Seed bulk metal included SS304 and SS316 (in cubes and 2- to 3-mm plate), Cu (5-mm busbar cut to ~2 × 4-cm lengths), Inconel plate (4 cm × 4 cm × 2 mm), and SS canisters with removable push-fit lids (cylindrical, with a diameter of 7.5 cm and a height of 15 cm).

In all cases, an inert atmosphere was maintained by evacuation to ~5E−2 mbar and backfill with 100 mbar Ar. The crucibles [either Zirconia (ZC93 1017) or alumina (AL68S 5050)] and liners (AL97 1017) used were supplied by Capital Refractories [11]. Power was increased in a stepwise approach until the melting point was reached (or it was determined that the melt would not be successful). Power and temperature were logged at 8-s intervals via the VIM control system. Each melting trial was conducted as a single replicate ($n = 1$).

Table 1 summarizes the key process parameters per melt. Plots of the power against time and temperature data sets are provided in the supplementary materials. The temperatures used were kept below the maximum use temperature for the crucibles and liners (~1800ºC), therefore the melting temperature of W was not reached in these trials.

Each melting trial was conducted as a single replicate ($n = 1$).

Visual melt success was assessed using a semiquantitative rubric (Table 2) with three criteria: consolidation C, surface integrity SI, and residual fines RF.

Scores were assigned by two independent reviewers; disagreements were resolved by consensus. A weighted combined score (0 to 5) was calculated, as shown in Eq. (2), to provide an overall indicator of melt success, where C is consolidation, SI is surface integrity and RF is residual fines,

$$(0.6 \times C) + (0.2 \times SI) + (0.2 \times RF) = Weighted\ Combined\ Score . \quad (2)$$

III. RESULTS

III.A. Pyrolyzer Heating

The average mass increases over the n replicates at 900°C for 2 h are detailed in Table 3.

The W oxidized in air formed yellow/green fibrous aggregates that originally agglomerated but fell back into a powder with handling and time. The Raman spectra result matched WO_3 (Fig. 2). The Ar-heated W showed a darker suboxide appearance consistent with WO_2, confirmed by Raman (Fig. 2).

SS formed a brittle cohesive mass in air and partial cohesion in Ar. Mixed W/SS exhibited overflow/expansion in air and cohesive agglomerates in Ar. Evidence of agglomeration is indicated in Fig. 3 through acquisition spectra and visual observations of W fibers on SS particles in Ar. This is exhibited to a lesser degree in air (Fig. 4) with small W oxide "spikes" on the SS grains.

Comparison micrographs between the pretest and the air and Ar tests for both SS and W are shown in Fig. 5.

The diameter and area increase measurements are given in Table 4, providing a qualitative indicator of morphology change.

III.B. MDF Dust Basket Trials

Loose dust, brittle agglomerates, and bolts showing warping due to thermal expansion and oxidation were observed. These effects are shown in Fig. 6.

Mass measurements over the runs are detailed in Table 5. The post-total masses (basket + dust) increased by +1.13% and +1.12%, respectively.

III.C. Vacuum Induction Melting

The complete results are presented in Table 6. For the SS swarf, complete melting required high seed bulk. The successful runs used bulk fractions of ~67% and ~79% by mass, while an ~50% bulk fraction yielded partial melting. The SS powder alone failed to melt and required adding ~10% to 20% bulk to complete melting. This included using a SS canister as the seed.

The W powder was incorporated into SS and Inconel ingots with some heterogeneity. The W-rich regions were seen at the base of the ingots. With Cu, W remained largely unconsolidated at the bottom of the crucible. The Cu phase mostly melted.

IV. DISCUSSION

IV.A. Pyrolyzer Heating

Morphology changes were assessed qualitatively using ImageJ via the diameter measurements and derived projected areas (Table 4). Both methods indicated substantial structural

TABLE 1

Key Process Parameters With Liners of AlL (AL97 1017), AlC (AL68S 5050), or ZrC (ZC93 1017)

Melt Identifier	Material	Swarf Mass (W) (kg)	Bulk Mass (kg)	Loading Procedure	Liner	Pyrometer Maximum (°C)	Melt Time (h/min/s)	Peak Power (kW)	Total Power (kWh)
1	SS swarf	0.51	0	Swarf only	AlL	964.16	01:29:19	12	9.75
2		0.46	0	Swarf only	AlL	986.47	01:31:25	12	3.99
3		0.4	1.5	~20% swarf, bulk at base	AlL	1523.39	00:54:35	12	5.13
4		0.49	0.94	~33% swarf, bulk at base	AlL	916.72	01:15:08	15	8.51
5		0.51	1.02	~33% swarf, bulk on top	AlL	1505.14	01:02:01	12	6.41
6		0.58	0.58	~50% swarf, bulk on top	AlL	1395.7	00:55:53	13	5.44
7		0.58	0.58	~50% swarf, bulk on top	AlL	1155.05	01:59:05	12	9
8		0.43	0.85	~33% swarf; bulk = 186 g tin + 662 g SS	AlL	1362.68	01:10:22	12	8.5
9		0.43	0.86	~33% swarf; bulk = 186 g tin + 678 g SS	AlL	1280.84	01:16:08	13	8.77
10a	SS powder	1	0	100% swarf	ZrC	–	–	–	–
10b		1	0.26	Single bulk piece buried in top 1/3	ZrC	1514.33	00:42:30	10	3.75
11		0.93	0.19	Loaded canister with powder	AlL	1499.94	00:45:00	12	4.3
12		1.66	0.19	Loaded canister with powder	AlL	1615.35	00:46:14	12	5.31
13	Cu	1	0	Cu pellets only	ZrC	1220.69	00:23:30	7	1.62
14	SS and W	0.90 (0.26)	0.13	Steel/W powders mixed in crucible, bulk steel on top.	ZrC	1502.96	00:45:50	10	4.97
15		0.00 (0.60)	2.4	Bulk steel loaded into crucible, W powder poured into base.	AlL	1606.76	00:58:07	14	8.07
16		0.90 (0.27)	0.19	Steel/W powders mixed in steel canister; lid replaced with equivalent mass of bulk steel	AlL	1615.74	00:45:28	13	5.34
17	Inconel and W	0.00 (0.60)	2.41	Bulk Inconel loaded into crucible; W powder in base.	AlL	1651.8	00:51:27	14	6.57
18	Cu and W	0 (0.3)	1.2	W dust loaded in base of crucible; bulk Cu on top.	AlC	1425.11	00:34:38	10	3.11
19		1 (0.25)	0	Cu pellet in base of crucible; W dust on top.	AlC	1420.91	00:32:23	10	2.81

TABLE 2

Rubric Defining Semiquantitative Visual Scoring Criteria for Melt Success

Criterion	Score 0 (Poor)	Score 1 to 2 (Low)	Score 3 to 4 (Moderate)	Score 5 (High)
Consolidation	No cohesion	Partial clumping	Majority fused	Fully consolidated ingot
Surface integrity	Fragmented, irregular edges	Large voids or severe roughness	Minor cracks, generally continuous surface	Smooth, continuous surface, no voids
Residual fines	Large amount of loose powder (>50%)	Moderate loose powder (10% to 50%)	Trace loose powder (<10%)	No visible loose powder

TABLE 3

Mass Increase Results for W, SS, and mixed W/SS Dust Heating Experiments

Dust	Gas	n	Mean Mass Increase (%)	Standard Deviation (%)	Standard Error (%)
SS	Air	3	3.93	0.33	0.19
	Ar	2	0.71	0.01	0.01
W	Air	3	24.83	0.9	0.51
	Ar	3	0.42	0.03	0.02
Mixed SS/W (40:60)	Air	1	21.14	–	–
	Ar	1	0.46	–	–
Mixed SS/W (60:40)	Air	1	28.65	–	–
	Ar	1	0.55	–	–

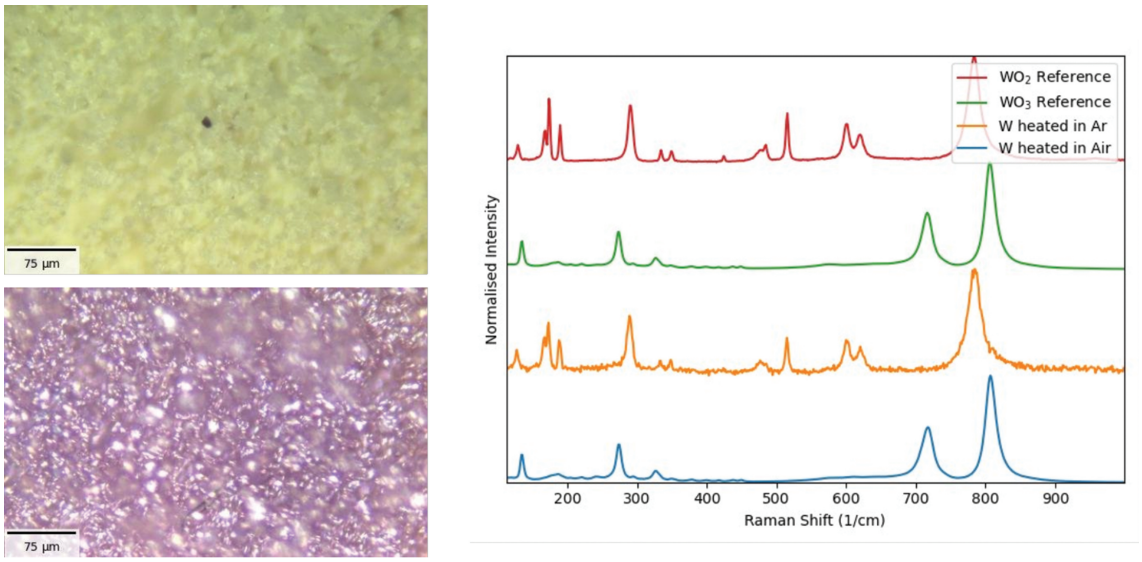

Fig. 2. Raman spectra identifying WO_2 and WO_3 in the W heated in air.

changes but did not scale with gravimetric oxygen uptake (Table 3). For SS, the mean diameter increased by 37% to 57%, while the ImageJ analysis showed area increases of ~254% (Ar) and ~1049% (air), consistent with agglomeration and porous overgrowth. For W, the diameter increased by 91% in air, yet ImageJ showed a 43% decrease in the

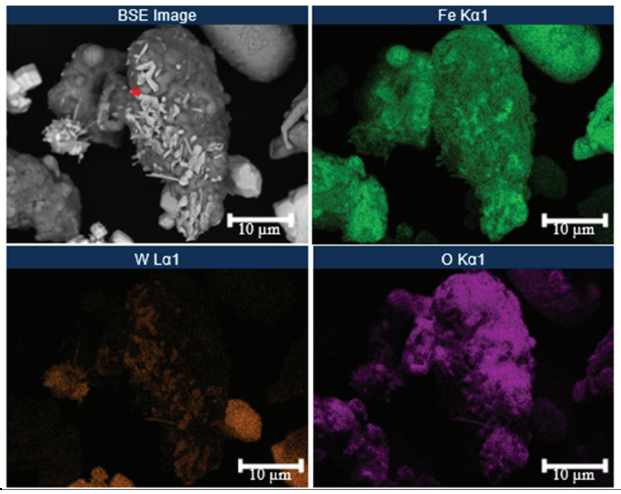

Spectrum Label	Composition (Weight %)							
	Fe	W	Cr	O	Ni	Mo	Si	Al
Map Sum Spectrum	38.8	21.5	19.6	14.4	*4.4*	*0.8*	*0.3*	*0.1*
Acquisition Spectrum	25.4	50.0	8.2	14.1	*2.2*	*0.0*	*0.0*	*0.0*

Fig. 3. Back-scattered electron and EDS images for dust mixture after heating in Ar (EHT = 20 kV, working distance = 8.5 mm, three frames) and accompanying compositions. The acquisition spectrum location is marked by the red X. Values below the detection limit for EDS (~5%) have been italicised to highlight their unreliability.

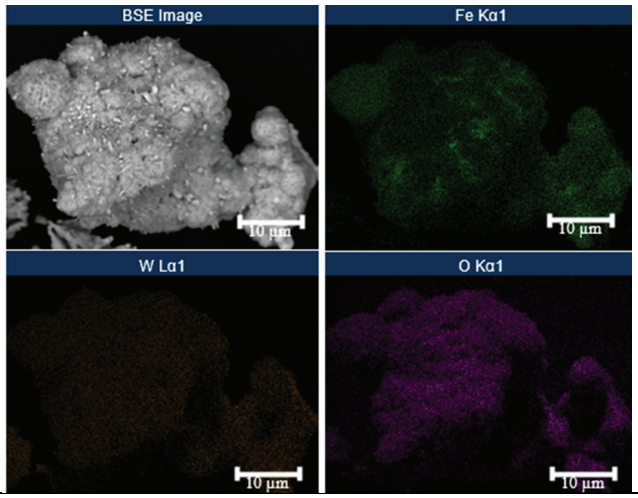

Spectrum Label	Composition (Weight %)					
	W	O	Cr	Fe	Mo	Na
Map Sum Spectrum	47.5	21.1	17.0	12.7	*1.2*	*0.4*

Fig. 4. Back-scattered electron and EDS images for dust mixture after heating in air (EHT = 20 kV, wd = 8.5 mm, three frames) and accompanying compositions. Values below the detection limit for EDS (~5%) are italicized due to their unreliability.

mean area due to the fragmentation into smaller oxide particles (seen in Fig. 6). These metrics, therefore, were treated as qualitative indicators of morphology change rather than quantitative measures of oxidation.

In mixed W/SS, the volume increase led to the sample boat overflowing at 900°C. In waste treatment contexts, this volume increase could lead to safety concerns when treating dust, as any overflow from the treatment vessel could be suspended in the interior of the oven or furnace. This would lead to an increased risk of process disruptions. For W it may also impact detritiation, where oxide layers could slow tritium release [8,9].

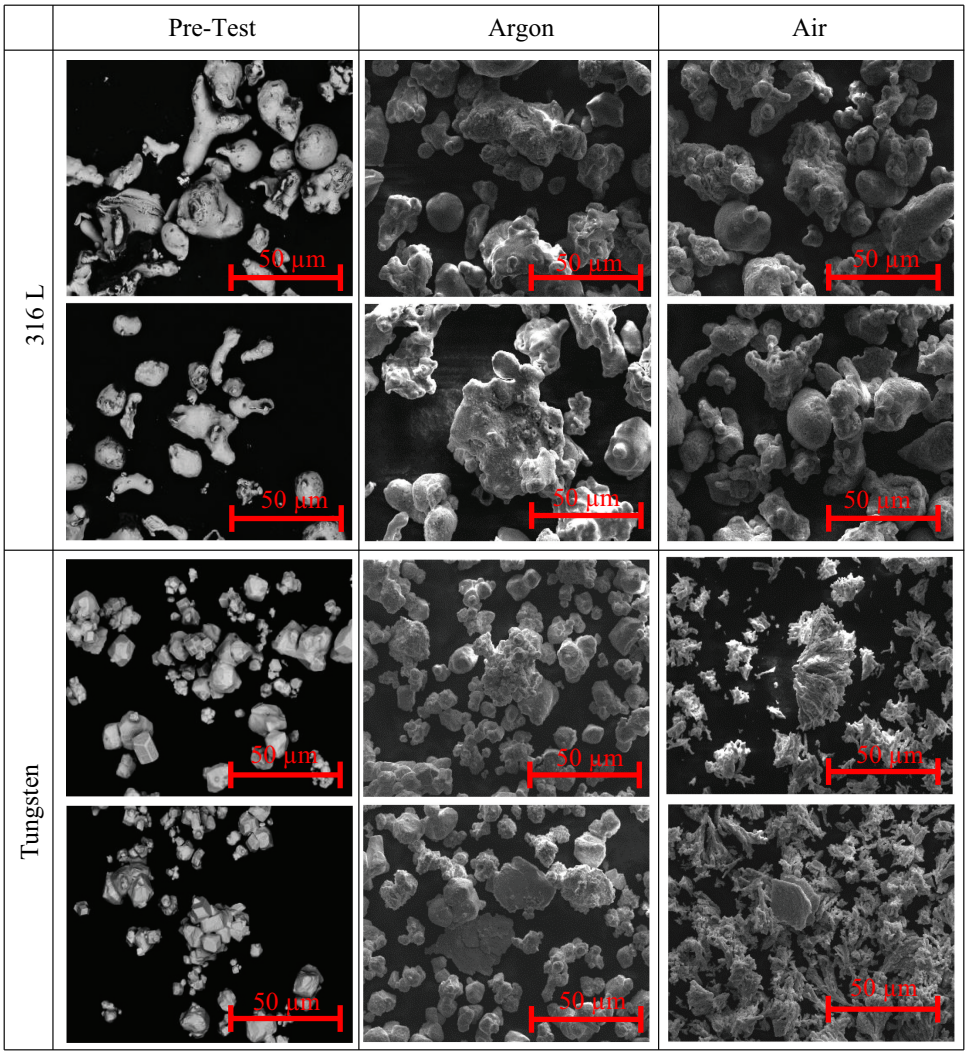

Fig. 5. Comparison micrographs for SS and W showing the particle size increase when heated in Ar and Air.

TABLE 4

Diameter ($N = 5$) and Area Measurements of W and SS Particles in the Pretest and the Ar and Air Tests

	Diameter (µm)			Area (µm^2)		
	Mean	Standard Deviation	Increase (%)	Mean	Standard Deviation	Increase (%)
Pre SS	21.48	6.45	–	191.31	203.28	–
SS Ar	29.52	11.93	37	677.90	851.22	254
SS Air	33.83	4.93	57	2198.53	2533.32	1049
Pre W	15.69	5.74	–	368.44	317.61	–
W Ar	17.32	6.53	10	733.69	805.48	99
W Air	30.05	15.12	91	210.57	376.23	−43

In Ar, the W dust darkened and WO_2 formed (likely due to small amounts of oxygen impurity in the pyrolyzer setup). This is not expected to affect safety considerations, but may still slow tritium release. While operational experience suggests that the detritiation of SS components is effective under oxidizing conditions, oxide growth during high-temperature exposure could increase the diffusion path length and reduce tritium release rates.

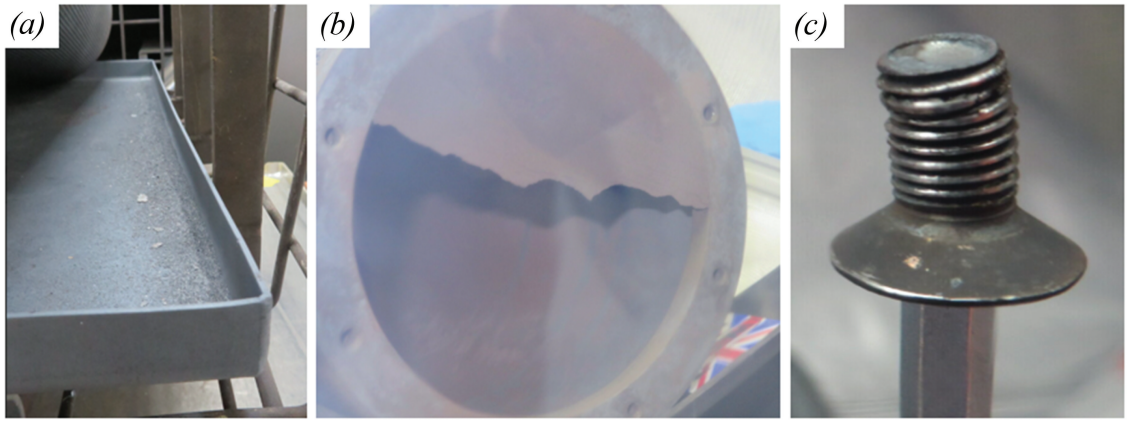

Fig. 6. (a) Loose dust in the metal tray, (b) dust that had agglomerated during treatment, and (c) a warped bolt.

TABLE 5

Mass Measurements for the Dust Baskets Pre and Post Treatment

Basket	Pre-Treatment Dust Mass (g)	Pre-Teatment Total Mass (g)	Post-Treatment Total Mass (g)	ΔTotal (g)
1 μm	997.6	5163.2	5221.6	58.4
5 μm	975.6	5246.0	5304.8	58.8

From the SEM and EDS evidence, the mechanism for adhesion in these trials was hypothesized to be early-stage sintering. This was supported by the elemental composition uniformity across the necked regions, as well as the smooth rounded necks between the particles, which is characteristic of diffusion-driven sintering rather than oxide bridging [12,13]. The effect of dust adhesion is discussed in Sec. IV.B.

IV.B. MDF Dust Basket Trials

Tray residues confirmed that some dust was lost throughout the process, which was hypothesized to be from thermal expansion allowing for the microscale dust to escape at the top and bottom seals. The mass of the tray residues was not measured during these trials.

For both baskets, the measured total mass of the basket plus dust increased by ~58 g. A positive change indicated that any dust loss during the run must have been more than offset by the oxidation gains of the dust and/or basket during the run, evaluated using a mass balance [Eq. (3)],

$$L = \Delta_{ox,dust} + \Delta_{ox,basket} - \Delta_{total}\,, \tag{3}$$

where Δ_{total} is the total mass gain (g), $\Delta_{ox,dust}$ is the dust oxidation gain (g), and $\Delta_{ox,basket}$ is the incremental oxidation gain from the run (g). This yielded a data only lower bound of $L \geq 0$.

$\Delta_{ox,dust}$ can be conservatively capped by taking the ~3.93% mass increase in the pyrolyser trials and equating it to ~40 g per kilogram of dust used during the trials. As the rate of air change within the MDF is much less than in the pyrolyser, and the dust was contained within the fine multilayer mesh, which would restrict O_2 renewal into the charge. $\Delta_{ox,dust}$ is expected to be at or below this cap.

The dust basket had already been oxidized from prior furnace exposure. Under diffusion-controlled oxidation, oxide growth follows a parabolic relationship [14]. Consequently, it was estimated that $\Delta_{ox,basket}$ would be small.

As we did not measure the basket-only oxidation (blanks) and the mesh construction parameters (wire diameters, porosity, and layer stack) were unavailable, $\Delta_{ox,basket}$ and $\Delta_{ox,dust}$ cannot be separated uniquely, and therefore a single numerical value for L was not identifiable from this data set. With $\Delta_{total} > 0$ in both runs, any dust loss evidenced in the tray must have been more than offset by oxidation gains, and the loss would be small relative to the starting dust charge.

Agglomeration was seen in the dust baskets, reducing the finely divided fraction, and thus, the handling and inhalation risks. These deposits required mechanical removal from

TABLE 6

Results for Particulate Melting Trials

Identifier		Swarf Mass (kg)	Bulk Mass (kg)	Observations	C	SI	RF	Score
SS swarf	1	0.51	0	Swarf fused but not melted	3	2	4	3
	2	0.46	0	Swarf fused but not melted	2	1	3	2
	3	0.4	1.5	Melt successful	5	4	5	4.8
	4	0.49	0.94	Overheated bottom of crucible due to swarf "bridge" on top	2	0	2	1.6
	5	0.51	1.02	Bulk on top of swarf melted down into ingot	5	4	5	4.8
	6	0.58	0.58	Partial melting of blocks suspended in swarf mesh	3	1	3	2.6
	7	0.58	0.58	Partial melting of blocks suspended in swarf mesh	4	2	3	3.4
	8	0.43	0.85	Consolidation and partial melting of canister and blocks	2	2	4	2.4
	9	0.43	0.86	Consolidation and partial melting of canister and blocks	3	2	4	3
SS powder	10a	1	0	No heating at all; removed after ~35 min, with reattempt with bulk (10 b).	0	0	0	0
	10b	1	0.26	Complete melting in good time and efficiency; small quantity of dust/flaked material collected.	5	4	3	4.4
	11	0.93	0.19	Complete melting in good time and efficiency	5	4	5	4.8
	12	1.66	0.19	Complete melting in good time and efficiency	5	4	5	4.8
Cu	13	1	0	Complete melting in good time and efficiency	5	5	5	5
SS and W	14	0.90 (0.26 W)	0.13	Almost no dust/flaked material inside the crucible	4	3	4	3.8
	15	0.00 (0.60 W)	2.4	Small quantity of dust/flaked material present in the bottom of the crucible; surface pitting.	4	3	3	3.6
	16	0.90 (0.27 W)	0.19	Almost no dust/flaked material inside the crucible; pits in the base revealed possible concentrations of solid powder.	4	3	4	3.8
Inconel and W	17	0.00 (0.60 W)	2.41	All the metal was consolidated, except for the small quantity of material ejected from the melt on to the sides of the liner.	4	3	3	3.6
Cu and W	18	0 (0.3 W)	1.2	Copper was melted into one solid piece although, not all of it had melted completely at the base; 0.26 kg W dust remained loose at bottom of the crucible.	3	4	0	2.6
	19	1 (0.25 W)	0	Copper was melted into one solid piece, although not all of it had melted completely at base of ingot; 0.17 kg W dust remained loose at bottom of the crucible.	3	2	0	2.2

the baskets. This can reduce throughput and may briefly re-aerosolize the fines during handling. Additionally, these deposits could occlude the mesh. For activated/tritiated dusts, agglomeration could be a net safety and disposability benefit, with an operational penalty that could be mitigated by developed remote removal techniques.

With larger dust sizes, it is expected that less to no dust would escape through the expansion gaps created, as well as less dust agglomeration. In the current configuration, this treatment method could be more suitable for treating dusts greater than micron scale. Further development on the dust baskets could also reduce the dust loss.

IV.C. Vacuum Induction Melting

The results showed that at 10 kHz, the powders and swarf below the skin depth δ coupled poorly. A bulk seed that coupled directly was required to form a melt bath, which then consolidated and melted the fine particles by inductive stirring and conduction. The results indicated that an approximately 10% to 20% bulk fraction is required for the fine dusts, with >66% required for the larger swarf. This was hypothesized to be due to the increased packing density of the finer material, and thus better thermal pathways.

The larger, 2- to 5-mm Cu granules melted easily without a seed required, as the size was much larger than the skin depth δ. If bulk metal was to be detritiated and size-reduced by melting, the dust and swarf could likely be used as infill material, with the bulk acting as a seed. Thus, melting would provide a convenient route to consolidate and detritiate this material without requiring additional processing steps. Further investigation is required to confirm these seed fractions due to the lack of replicates.

Another strategy proposed for handling and processing metallic dusts was containment and melting inside metal canisters. The motivation for this work was to minimize the exposure hazards of tritiated dusts that could occur during handling, transport, and treatment. The work performed with the SS canisters indicated the potential of this method, with up to 1.662 kg of SS powder melted using just the mass of the canister to seed the melting.

The SS and Inconel melts resulted in one consolidated ingot without visible loose W powder in most trials. Microstructural homogeneity remained unclear, but macroscale observations showed some minor cracking, pits, and other deformations in the ingots, as well as concentrations of W powder that consolidated but did not melt.

At 20 wt%, W is theoretically soluble in α-Fe [15]. It was expected that the mixing would enable dissolution into the Fe during the liquid phase and/or diffusion into α-Fe during the cooling phase if any solid W remained. The remaining W powder was hypothesized to be due to a lack of homogeneity throughout the mix and insufficient melt time during which the W could be incorporated.

For Inconel with W dust, few small particles were observed to eject from the melt. It was assumed that these were W particles being ejected by the stirring and heat from the melt, but no further testing was performed to confirm their composition. With further testing using different melt conditions, the ejection of these dusts could be minimized. Despite this, the resultant melt showed W dusts incorporated into the ingot.

The inclusion of W powder inhibited the melting of Cu, and the melts demonstrated very limited mixing and consolidation, with remnants of the original charge geometry visible and 87% and 68% of the starting W mass loose at the end of melts 18 and 19, respectively. It was hypothesized that the partial incorporation reflected mechanical entrapment rather than alloying, consistent with the W-Cu phase diagram [16,17], which shows negligible solubility. The increase in W density caused the powder to settle at the crucible base, which could have created a heat sink and impeded the full melting of Cu, providing an explanation as to why the Cu failed to fully melt at the base of the ingot.

V. CONCLUSION

The effective management of fusion dust waste is critical to minimize radiological hazards to operators and public, prevent environmental contamination, and ensure compliance with disposal regulations for the decommissioning of nuclear fusion reactors. At UKAEA, two methods of treatment of this dust have been inactively trialed, testing the methodology of baking and consolidating the dust into ingots via metal melting. The results are as follows:

1. The thermal processing trials significantly altered the dust characteristics through oxidation and agglomeration, which could impact post-operational waste handling and detritiation.

2. The dust containment baskets trials in the MDF showed promise for high-temperature processing with reduced contamination risk, though some limitations,

such as dust escape and agglomeration, require further testing and optimization.

3. The VIM results suggested the successful incorporation of micron-scale dusts into ingots utilizing small amounts of bulk material to induce the melt, reducing their dispersibility and offering a potential detritiation method simultaneously.

4. The bulk fraction thresholds for effective induction melting were indicated: fine powders required 10% to 20% bulk seed, while larger swarf may require up to 66% bulk for successful consolidation.

5. The metal canister trials indicated that they served as an effective methodology for containing, transporting, and treating particulate wastes via VIM while acting as the seed material.

6. The W dusts can be successfully incorporated into the SS dust, bulk, and Inconel bulk material, although incorporation issues were present when mixing W dusts in Cu-based melts due to poor miscibility.

7. Future research will focus on investigating the detritiation potential for dust material using these techniques while optimizing the methodology used, helping to develop these technologies into scalable treatment methodologies for dust wastes, ensuring the sustainability and safety of fusion energy deployment.

Acknowledgments

This work was carried out in collaboration with the TAL and MDF and Fusion Technology Facility at UKAEA, whose teams provided equipment, expertise, and time for carrying out these experiments safely and reliably. Raman spectroscopy was undertaken at Imperial College London by the Materials Division at UKAEA.

The pyrolyser heating work was partly funded by and undertaken in collaboration with the ITER project.

The MDF dust basket trials were undertaken as part of the Titans programme and funded by the European Union. The views and opinions expressed, however, are those of the authors only and do not necessarily reflect those of the European Union or the European Atomic Energy Community. Neither the European Union nor the granting authority can be held responsible for them.

The VIM work was undertaken in collaboration with EUROfusion. The views and opinions expressed, however, are those of the authors only and do not necessarily reflect those of the European Union or the European Commission. Neither the European Union nor the European Commission can be held responsible for them.

Many thanks for the support of these organizations.

Author Contributions

CRediT: **Thomas Stokes:** Conceptualization, Data curation, Investigation, Methodology, Supervision, Validation, Visualization, Writing – original draft, Writing – review & editing; **William Grove:** Investigation, Methodology, Supervision, Writing – original draft, Writing – review & editing; **James Hall-Bromley:** Validation, Writing – review & editing; **Daniella Heristchian:** Data curation, Formal analysis, Validation, Visualization; **Stephen Reynolds:** Funding acquisition, Resources, Writing – review & editing.

Disclosure Statement

No potential conflict of interest was reported by the author(s).

Supplementary Material

Supplemental data for this article can be accessed online at https://doi.org/10.1080/15361055.2025.2605607.

ORCID

Thomas Stokes http://orcid.org/0009-0000-4460-2693

References

1. F. G. Cesari et al., "Contaminated Metal Components in Dismantling by Hot Cutting Processes," *Proc. Int. Conf. on Nuclear Engineering*, Florida (2006); https://proceedings.asmedigitalcollection.asme.org.
2. L. Bonavigo et al., "Radioactivity Release and Dust Production During the Cutting of the Primary Circuit of a Nuclear Power Plant: The Case of E. Fermi NPP," *Prog. Nucl. Energy*, **52**, *4*, 359 (May 2010); https://doi.org/10.1016/j.pnucene.2009.07.009.
3. M. A. Ebadian, S. K. Dua, and C. H. P. H. Guha, "Size Distribution and Rate of Production of Airborne Particulate Matter Generated During Metal Cutting," Hemispheric Center for Environmental Technology, Florida International University (2001); https://www.osti.gov/servlets/purl/793521.
4. A. Vankrunkelsven, K. Dylst, and Y. D'Joos, "Tritium Release during Different Decommissioning Techniques," *Fusion Sci. Technol.*, **81**, *4*, 294 (2024); https://doi.org/10.1080/15361055.2024.2361198.

5. F. Larese Filon et al., "Skin Absorption of Metals Derived from Hydrogenated Stainless Particles in Human Skin: Results from the TITANS Project," *Environ. Pollut.*, **364**, 125327 (Jan. 2025); https://doi.org/10.1016/j.envpol.2024.125327.

6. E. L. Vernon et al., "Bioaccumulation, Release and Genotoxicity of Stainless Steel Particles in Marine Bivalve Molluscs," *Chemosphere*, **303**, 134914 (Sep. 2022); https://doi.org/10.1016/j.chemosphere.2022.134914.

7. M. Kresina et al., "Preparation for Commissioning of Materials Detritiation Facility at Culham Science Centre," *Fusion Eng. Des.*, **136**, 1391 (Nov. 2018); https://doi.org/10.1016/j.fusengdes.2018.05.019.

8. T. Stokes et al., "Detritiation of JET Beryllium and Tungsten," *Fusion Sci. Technol.*, 80, 479 (June 2023); https://doi.org/10.1080/15361055.2023.2219826.

9. M. Brenna, E. Petraglia, and F. Campi, "Detritiation of Graphite and Beryllium Plasma Facing Components," *The 19th SOFT*, Lisboa, Portugal, September 16, 1996 (1996).

10. H. A. Haus and J. R. Melcher, *Electromagnetic Fields and Energy*, Prentice Hall, Englewood Cliffs, NJ (1989); https://web.mit.edu/6.013_book/www/book.html (accessed Oct. 14, 2025).

11. "Crucibles and Related Products," Capital Refractories (Apr. 2013).

12. M. R. Mazlan et al., "Necking Mechanism Under Various Sintering Process Parameters—A Review," *Elsevier Editora Ltda*, **23**, 2189 (Mar. 1, 2023); https://doi.org/10.1016/j.jmrt.2023.01.013.

13. R. M. German, "Thermodynamic and Kinetic Treatments," *Sintering*, **2014**, 183 (Jan. 2014); https://doi.org/10.1016/B978-0-12-401682-8.00007-0.

14. S. Chandra-Ambhorn, T. Thublaor, and C. Pascal, "Chapter 1 Thermodynamics and Kinetics of the High Temperature Oxidation of Stainless Steels," *High Temperature Corrosion of Stainless Steels: An Alain Galerie Festschrift*, *in Solid State Phenomena*, Vol. 300, p. 1–24, Trans Tech Publications Ltd., Switzerland (Oct. 2020); https://doi.org/10.4028/www.scientific.net/SSP.300.1.

15. O. K. von Goldbeck, "Fe-W Iron-Tungsten," *Iron—Binary Phase Diagrams*, p. 164–167, Springer Berlin Heidelberg, Berlin, Heidelberg (1982); https://doi.org/10.1007/978-3-662-08024-5_76.

16. M. Vijayakumar, A. M. Sriramamurthy, and S. V. Nagender Naidu, "Calculated Phase Diagrams of CuW, AgW and AuW Binary Systems," *Calphad*, **12**, *2*, 177 (Apr. 1988); https://doi.org/10.1016/0364-5916(88)90019-3.

17. M. Hussain et al., "A Review on the Additive Manufacturing of W-Cu Composites," *Multidiscip. Digit. Pub. Inst. (MDPI)*, **15**, *2*, 197 (Feb. 1, 2025); https://doi.org/10.3390/met15020197.